"Superductile" Semicrystalline ABC Triblock Copolymers with the Polystyrene Block (A) as the Matrix

V. Balsamo*

Grupo de Polímeros USB, Universidad Simón Bolívar, Departamento Ciencia de los Materiales, Aptdo. 89000, Caracas 1080-A, Venezuela

F. von Gyldenfeldt and R. Stadler*

Makromolekulare Chemie II, Universität Bayreuth, 95440 Bayreuth, Germany

Received September 18, 1997; Revised Manuscript Received October 2, 1998

ABSTRACT: The relationship between the microphase morphology and stress−strain behavior of a polystyrene-*block*-polybutadiene-*block*-poly(ϵ-caprolactone) SBC triblock copolymer has been investigated with polystyrene as the major component. The semicrystalline PCL block does not change significantly the basic morphology, but it affects the form of the microdomains, so that $S_{57}B_{27}C_{16}$ shows a "polygonal" core shell morphology in a PS matrix. This morphology seems to be the consequence of crystallization in the inner PCL cylinders inducing deformation of the microdomains, which may create interfacial stresses. These stresses can generate small microcrazes upon external loading which may be responsible for the high elongations at break in this material. Moreover, the long-range order of the microdomains, which can be affected through the preparation conditions, determines the stress−strain behavior. Copolymers with 57 and 51 wt % PS and a corresponding "PS matrix" exhibit elongations at break up to ∼800%.

Introduction

The fascinating ability of block copolymers to self-assemble into a variety of organized structures has been the subject of many investigations. The formation of a large number of new mesophase structures in amorphous ternary block copolymers (ABC block copolymers) is well documented both experimentally and theoretically.[1−8] In contrast to binary block copolymers (AB, ABA) in the strong segregation limit, where the composition is the main variable which determines the equilibrium microphase morphology, the morphology of ABC triblock copolymers is governed not only by two independent composition variables (ϕ_A, ϕ_B, $\phi_C = 1 - \phi_A - \phi_B$) but also by the balance of three interaction parameters (χ_{AB}, χ_{AC}, χ_{BC}) which may be expressed alternatively by their interfacial tensions (γ_{AB}, γ_{AC}, γ_{BC}). As a consequence, chain topology (ABC, BAC, ACB) is of key importance.[5,6]

The morphologies of amorphous symmetric ABC triblock copolymers in the strong segregation limit have been well described by a simple thermodynamic model[5] based on a Flory−Alexander−deGennes−Semenov approach.[9,10] The same approach has been applied successfully on asymmetric ABC triblock copolymers.[7,11−13] One class of morphologies in asymmetric ABC triblock copolymers has structures where cylinders are packed in a matrix. A variety of cylindrical ABC morphologies can be envisaged. In general, they can be divided into two groups, where either one of the end blocks or the center block forms the matrix. If B is the major component, A and C cylinders may be formed in a B matrix.[14−16] For amorphous triblock copolymers where one of the end blocks forms the matrix (for example A), the sum ($\phi_B + \phi_C$) will define whether a cylindrical or a spherical morphology is formed, and the ratio of the volume fraction ϕ_C/ϕ_B and the thermodynamic balance will govern the type of cylindrical structure that will be created.[7] Variations of the block type and sequence may alter the details of this morphological picture. If one or more of the blocks are able to crystallize, a much more complex behavior will be expected because of the interplay of crystallization and microphase separation.

It has been shown for semicrystalline AB diblock copolymers that the microphase morphology is influenced by a strong coupling of crystallization and microphase separation.[17−19] The crystallization process could either disturb an already organized structure, inhibit the organization of microphases, or induce a transition between two different morphologies. At the same time, the presence of amorphous blocks could affect the crystallization process. Previous studies on ABC triblock copolymers with crystallizable blocks are limited to the recently reported high molecular weight polystyrene-*block*-polybutadiene-*block*-poly(ϵ-caprolactone) (SBC) triblock copolymers,[20] where the C-block can crystallize, and their hydrogenated versions, where the B- and C-blocks can crystallize.[21,22] Balsamo et al.[23] demonstrated that the crystallization process of the poly(ϵ-caprolactone) (PCL) block is affected by the presence of the amorphous blocks. A general decrease of the crystallinity as well as the occurrence of fractionated crystallization is observed, especially for those copolymers with low PCL content. Due to the low PCL content, PCL forms a dispersed phase, whose average size is so small that the number of particles is much greater than the number of active heterogeneities usually present in this polymer. Therefore, crystallization takes place with more than one exotherm, and that is precisely what it is termed "fractionated crystallizaton".[23−28]

To demonstrate the effect of the crystallizable block on the morphology in the SBC triblock copolymers, we report here the microphase morphology of a copolymer with polystyrene as the major component. Besides the morphological description, the stress−strain behavior will be discussed. While considerable work deals with the morphology of amorphous block copolymers, there has been less research on the relationship of the

10.1021/ma971380k CCC: $18.00
Published on Web 02/02/1999

mechanical properties with the morphology, especially in the case of ABC triblock copolymers. Argon et al.[29,30] studied the formation of crazes in PS-*b*-PB AB diblock copolymers as a function of the morphology and showed that cylindrical PB microphases in a PS matrix can generate materials that behave similar to rubber modified polystyrenes. Ph. Teyssié et al.[31] investigated the stress−strain behavior of PS-*b*-PCL diblock copolymers. They found, as expected, that the mechanical behavior of PS-*b*-PCL copolymers changes dramatically when phase inversion occurs, i.e., when the nature of the continuous phase changes. On the other hand, when the minor component forms semicontinuous phases intermingled within the matrix of the major block, there is evidence of a strong dependence of the stress−strain behavior on the two-phase morphology. Extensive studies have been performed on the mechanical properties of ABA copolymers and in particular on polystyrene-*block*-polybutadiene-*block*-polystyrene SBS triblock copolymers.[32−37] SBS with low PS content behaves similarly to a cross-linked conventional rubber. On increasing the PS content, the SBS shows a yielding process with neck formation followed by cold drawing and then an elastic extension. This process occurs with a continuous rodlike or platelike endblock.[36,37] It has been reported that crazing and shear yielding are present in these cases. At high endblock concentrations, the plastic phase (PS) is continuous, and the dispersed midblock phase (spheres or cylinders) produces a system resembling high impact polystyrene. In these cases, crazing has been proposed as the main fracture mechanism.[32,33] Nevertheless, Nomura et al.[34] have shown neck propagation in a SBS with PB cylinders dispersed in a PS matrix. In the case of ABC triblock copolymers the studies of the mechanical properties have been limited to the amorphous ones.[38−40] Basically, it has been reported that the block that conforms the matrix controls the mechanical properties of the triblock copolymers. As far as the authors are aware, there are no reports on the mechanical properties of semicrystalline ABC triblock copolymers in the literature. In the present paper we will focus on the relationship between the morphology, crystallization, and mechanical properties of polystyrene-*block*-polybutadiene-*block*-poly(ϵ-caprolactone) SBC triblock copolymers, where the PCL block can crystallize and where PS is the major component.

Experimental Section

The SBC triblock copolymers and the poly(ϵ-caprolactone) homopolymer used in the present study were prepared by sequential anionic polymerization in benzene. *sec*-Butyllithium was used as initiator, and 1,1-diphenylethylene (DPE) was added as capping agent for the crossover reaction from polybutadienyl anions to ϵ-caprolactone. The reaction time of this last monomer was strictly controlled to prevent side reactions such as backbiting. The details of the synthesis are described elsewhere.[20] The molecular characteristics of the materials are presented in Table 1. The molecular weight of the PS precursors and the molecular weight distribution of all polymers were determined by gel permeation chromatography in THF (calibrated with PS standards). The composition and molecular weight of the copolymers were determined by ^{1}H NMR spectra.

Films (thickness ~1 mm) of the block copolymers were slowly cast at room temperature from 5 wt % toluene solutions. For further equilibration the dry films were annealed at 140 °C for 2 h under nitrogen atmosphere. Longer annealing times did not affect the morphology.[41] The samples were then cooled to a selected crystallization temperature T_c where they were kept for ~5 h. Finally, they were quenched to 25 °C. Another set of samples was melt-pressed at 180 °C under vacuum and then quenched in cold water. Ultrathin sections (~40 nm) of the block copolymers were obtained at −120 °C using a FC4 Reichert Ultramicrotome equipped with a diamond knife. The ultrathin sections were stained using osmium tetroxide under vacuum at room temperature. The morphology was studied by transmission electron microscopy (TEM) using a Philips transmission microscope operating at 80 kV.

The stress−strain behavior of the materials was investigated using 0.1−0.3 mm thick samples, which were prepared in a similar way as for transmission electron microscopy (solution cast or melt pressed). The samples had a rectangular form with the following dimensions: 4.0 cm × 0.6 cm. The measurements were performed at 40 mm/min using a gauge length of 2.0 cm with a home-built stress−strain machine (500 N cell). An isolated temperature chamber was coupled to the machine in order to make measurements at temperatures higher than room temperature. Each reported value represents the mean value of at least four independent measurements.

Table 1. Molecular Characteristics of the Materials and Volume Fractions of the Components in the SBC Triblock Copolymers

polymer[a]	$M_n \times 10^{-3}$/ g mol^{-1}	M_w/M_n	ϕ_S	ϕ_B	ϕ_C	PB % 1,4	PB % 1,2
PCL	83	1.50			1.00		
$S_{57}B_{27}C_{16}$	137	1.12	0.55	0.30	0.15	91	9
$S_{51}B_{09}C_{40}$	105	1.10	0.50	0.08	0.42	88	12

[a] The subindices represent the weight percent of each component.

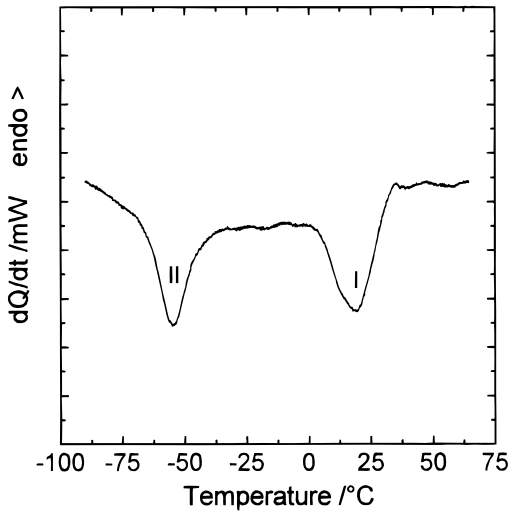

Figure 1. DSC cooling scan of $S_{57}B_{27}C_{16}$ recorded at −20 °C/min.

Results and Discussion

In our previous work we demonstrated through differential scanning calorimetry that $S_{57}B_{27}C_{16}$ is microphase separated into a PS, PB, an amorphous, and a crystalline PCL phase and that the PCL block crystallizes in a fractionated fashion (see exotherms I and II in Figure 1).[23] The reduction of the melting point of the PCL in the block copolymer (52 °C), obtained from dynamic DSC scans, is not very pronounced compared to pure PCL (56 °C).[23] In contrast to other SBC triblock copolymers with a PCL content higher than 36 wt %, this block copolymer does not show any crystalline spherulitic superstructure in the optical microscope. On the basis of these observations, we assumed that the microphase morphology should not be significantly

Table 2. Interaction Parameters (χ_{12}) and Interfacial Tensions (γ_{12}) of the SBC System

polymer pair	PS/PB	PB/PCL	PS/PCL
χ_{12}[a]	0.0623	0.1315	0.0118
γ_{12}/dyn cm^{-1} [b]	2.00	2.86	0.86

[a] Calculated from the solubility parameters[41,42] $\delta_S = 9.1$ (cal/cm^3)$^{1/2}$, $\delta_B = 8.4$ (cal/cm^3)$^{1/2}$, $\delta_C = 9.4$ (cal/cm^3)$^{1/2}$ under the assumption that the molar segmental volumes are given by the geometric mean of the molar volumes of the components according to $\chi_{12} = (V_s/RT)(\delta_1 - \delta_2)^2 = (N_A a^3/RT)(\delta_1 - \delta_2)^2$ with V_s = mean molar segmental volume, $T = 25$ °C, and a = Kuhn step length ≈ 0.5 nm. [b] Surface tensions calculated at 150 °C according to $\gamma_{12} = (kT/a^2)(\chi_{12}/6)^{1/2}$.

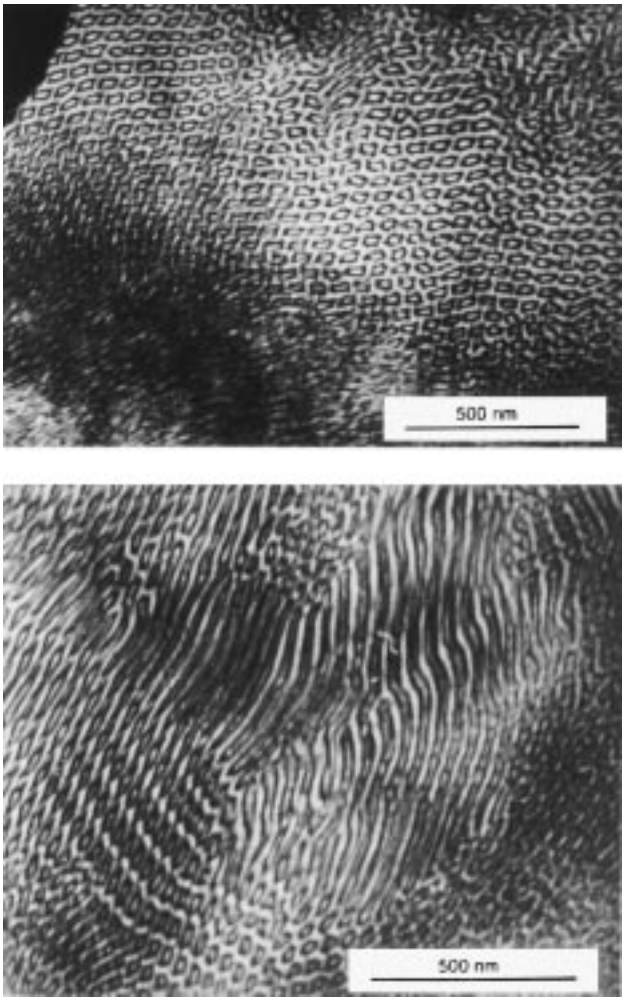

Figure 2. Transmission electron micrographs of $S_{57}B_{27}C_{16}$ cast from toluene solutions and annealed at 140 °C for 2 h (stained with OsO_4).

affected in comparison to what we would expect for amorphous ABC triblock copolymers.

Table 2 lists the Flory−Huggins interaction parameters (χ_{12}) and interfacial tensions (γ_{12}) for the respective pairs in the SBC triblock copolymers calculated from the middle Scott−Hildebrandt solubility parameters δ. A comparison of these values shows that the incompatibility increases in the serie PS/PCL ≪ PS/PB < PB/PCL. For this thermodynamic balance and the sequence $\phi_C < \phi_B < \phi_S$ and $(\phi_C/\phi_S) < 1$, a cylindrical core shell morphology is expected[7] for $S_{57}B_{27}C_{16}$ with a PCL core in a PB shell in a PS matrix.

Figure 2a shows a TEM micrograph of the $S_{57}B_{27}C_{16}$ triblock copolymer ($\phi_C/\phi_B = 0.5$) stained with OsO_4. Due to the staining conditions, PS appears gray as the matrix forming component. PB can be recognized as an *edge-shaped* black shell around bright cores of also irregular-shaped PCL. This morphology corresponds to a perpendicular view of the core shell morphology but with a shape not reported before. Microdomains, which were cut parallel to their main axis, are also observed as a layered structure of PS, PB, and PCL in Figure 2b. On the basis of these observations, we can conclude the formation of *core shell polygonal cylinders* which in analogy to our previous work will be designated as "pc_ic" (polygonal cylinder in cylinder). A schematic representation of the hexagonal array of this morphology is shown in Figure 3.

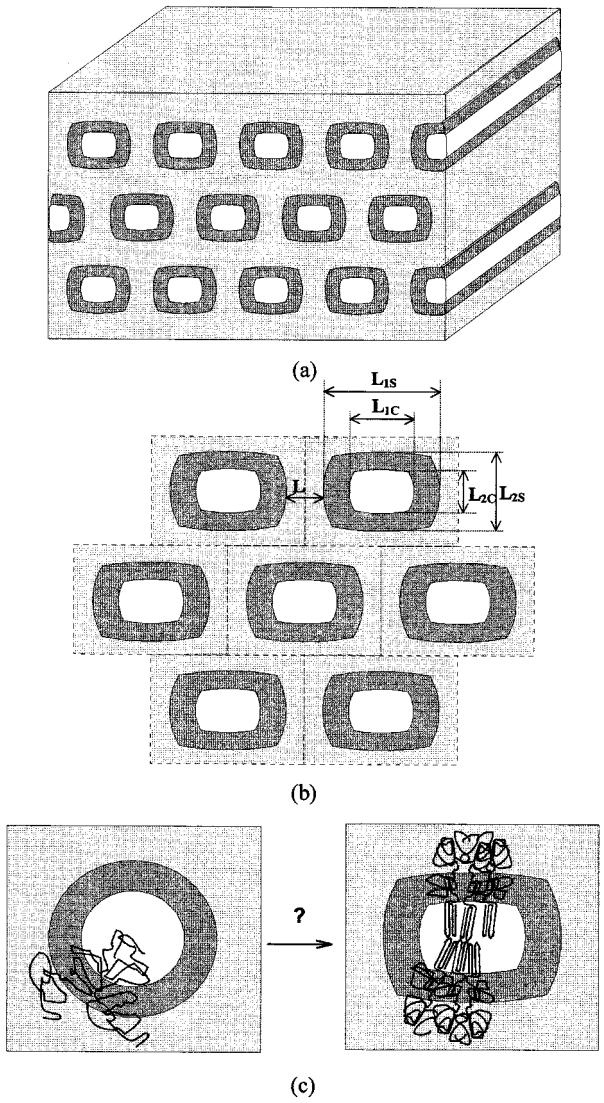

Figure 3. (a) Schematic representation of the *core shell polygonal morphology "pc_ic"*. (b) Dimensions of the microdomains in the selected orthorhombic unit cell. (c) Transition from circular cylinders to cylindrical polygons, supposedly due to the crystallization of the core.

In contrast to the core shell cylinders observed for amorphous triblock copolymers of similar composition, the cylinders in $S_{57}B_{27}C_{16}$ have an unusual polygonal shape which could be due to the deformation of circular-shaped cylinders during the crystallization process of the inner PCL cylinder, despite of the glassy PS matrix at the crystallization temperature. The PCL block shows a crystallinity of 38%.[23] Therefore, it can be concluded that although the semicrystalline core does not change the expected basic morphological motif when the PCL

Table 3. Experimental and Calculated Dimensions of the Cylindrical Polygons of $S_{57}B_{27}C_{16}$[a]

$S_{57}B_{27}C_{16}^{137}$, $T_c = 42$ °C					
	L_{1S}/nm	L_{2S}/nm	L_{1C}/nm	L_{2C}/nm	L/nm
measd	47.3 ± 2.4	29.0 ± 4.6	30.2 ± 5.7	13.0 ± 3.5	14.4 ± 1.6
calcd	44.1	27.4	25.6	15.7	

[a] S = shell, C = core.

is the minor component, it can affect the shape of the microdomains.

Table 3 summarizes the dimensions of the core shell morphology as obtained from TEM. Besides the polygonal form of the cylinders, a pronounced asymmetry of the microdomains ($L_{1S} > L_{2S}$) can be deduced from TEM (S = shell, C = core). This might be attributed to the lamellar shape of the crystals in the core (see Figure 3c). At present we do not know how the PCL crystals are oriented within the inner cylinder.

Due to the polygonal form of the cylinders, an orthorhombic cell (see Figure 3b), which approximates the symmetry of this system, was selected for the calculation of the dimensions of the microdomains. Based on the L_{1S} and L_{2S} dimensions as the parameters obtained from TEM with the highest accuracy, the area A and the asymmetry a of the unit cell can be calculated.

$$A = (L_{2S} + L)(L_{1S} + L) \tag{1}$$

$$a = \frac{L_{1S} + L}{L_{2S} + L} \tag{2}$$

We obtained from TEM data that the vertical spacing of the polygonal cylinders is approximately the same as the horizontal spacing between the microdomains. From eqs 1 and 2 and the volume fractions of the block components the dimensions of the polygons were calculated.

$$L_{2C} = \sqrt{\frac{\phi_{PCL}A}{a}} \tag{3}$$

$$L_{1C} = aL_{2C} \tag{4}$$

$$L_{2S} = \sqrt{\frac{(\phi_{PB} + \phi_{PCL})A}{a}} \tag{5}$$

$$L_{1S} = aL_{2S} \tag{6}$$

The comparison between these calculated dimensions and the values obtained from TEM is quite remarkable (Table 3).

The morphology of this block copolymer has a pronounced influence on the mechanical behavior. Figure 4 shows the stress−strain curves of $S_{57}B_{27}C_{16}$ cast from toluene solutions (S) after the equilibration treatment. The small strain behavior is dominated by the component, which constitutes the matrix phase (PS), however, with a strong modification that can be related to the presence of the other blocks. The data are summarized in Table 4.

The chemical linkage between the blocks provides the possibility of an efficient stress transfer between the microphases. This phenomenon was investigated in detail by Argon et al.[29,30] in their study of craze formation and propagation in PS-*b*-PB diblock copolymers. A strong whitening of the specimens during the loading process indicates the formation and propagation of crazes through the sample. These crazes are a consequence of preexistent internal surface stresses, which emerge during the solidification of the components. For PS-*b*-PB diblock copolymers with PB cylinders in a PS matrix elongations similar to those of rubber modified polystyrenes (∼50%) were found. Also for SBS triblock copolymers with a spherical or cylindrical PB domain morphology, crazing has been proposed as the main fracture mechanism.[33] The same explanation can be applied to our material. Moreover, it can be speculated that the polygonal form of the core shell cylinders (see previous section) could facilitate the initiation of crazes from the corners as will be discussed later. Since Teyssié et al.[31] reported that PS-*b*-PCL diblock copolymers with a PS matrix showed a brittle behavior ($\epsilon_b \sim 20\%$), it seems likely that the rubbery PB shell is a prerequisite to achieve the observed toughness in $S_{57}B_{27}C_{16}$ (S).

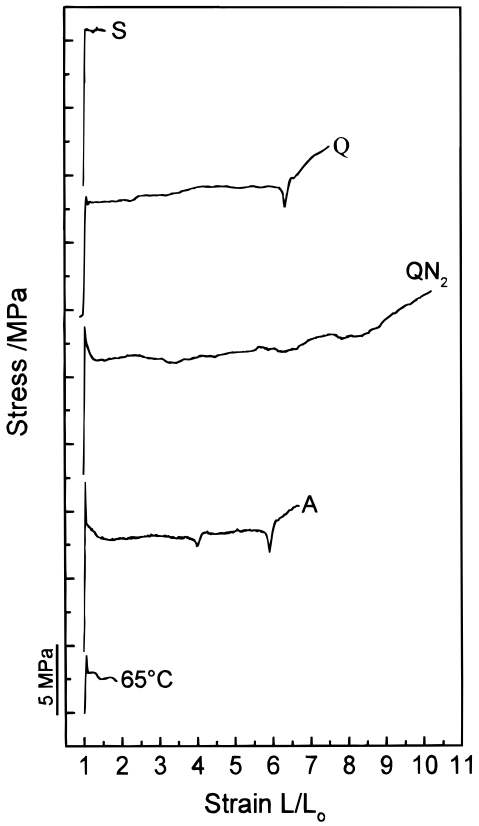

Figure 4. Stress−strain curves of $S_{57}B_{27}C_{16}$ prepared under different conditions (40 mm/min): S = solution cast; Q = quenched in cold water; QN_2 = quenched in cold water and after immersed in liquid nitrogen; A = annealed at 140 °C for 2 h; 65 °C = measured at 65 °C.

In addition to the stress whitening (most likely due to crazing) neck formation was observed. It indicates a combination of the processes of craze formation and propagation and shear yielding, similar to the results found by Nomura et al.[34] in a SBS with PB cylinders and 56 wt % PS.

In practical applications thermoplastic elastomers are normally processed from the melt and not from solution. Therefore, we studied the influence of the preparation conditions on the stress−strain behavior of $S_{57}B_{27}C_{16}$. For comparison $S_{51}B_{09}C_{40}$, which also has a PS matrix, was studied. A series of samples were compression molded and quenched into cold water (Q). Figure 4 and

Table 4. Stress−Strain Properties of $S_{57}B_{27}C_{16}$ and $S_{51}B_{09}C_{40}$, Prepared under Various Conditions[a]

preparation conditions	E/MPa	σ_y/MPa	ϵ_y/%	σ_b/MPa	ϵ_b/%
$S_{57}B_{27}C_{16}$					
cast from toluene solutions (S)	715 ± 85	14.6 ± 2.9	3.1 ± 1.8	8.4 ± 1.2	58 ± 11
quenched in cold water (Q)	246 ± 74	9.4 ± 0.9	5.0 ± 1.4	9.8 ± 2.0	690 ± 104
quenched, annealed (A)	352 ± 164	9.8 ± 1.8	2.8 ± 1.0	8.7 ± 1.8	455 ± 154
quenched in liquid nitrogen (QN_2)	317 ± 60	14.4 ± 0.7	5.5 ± 2.1	15.9 ± 2.1	890 ± 98
measurement at 65 °C	173 ± 24	4.8 ± 0.4	5.1 ± 0.2	2.0 ± 0.1	40 ± 34
$S_{51}B_{09}C_{40}$					
quenched in cold water (Q)	265 ± 42	11.5 ± 2.3	6.0 ± 0.9	17.4 ± 1.2	730 ± 104
quenched in liquid nitrogen (QN_2)	316 ± 53	13.2 ± 0.9	7.0 ± 1.7	16.7 ± 2.1	870 ± 98
polystyrene[44]	2000			40	3

[a] E = modulus, σ_y = stress at the yield point, ϵ_y = elongation at yield point, σ_b = stress at break, ϵ_b = elongation at break.

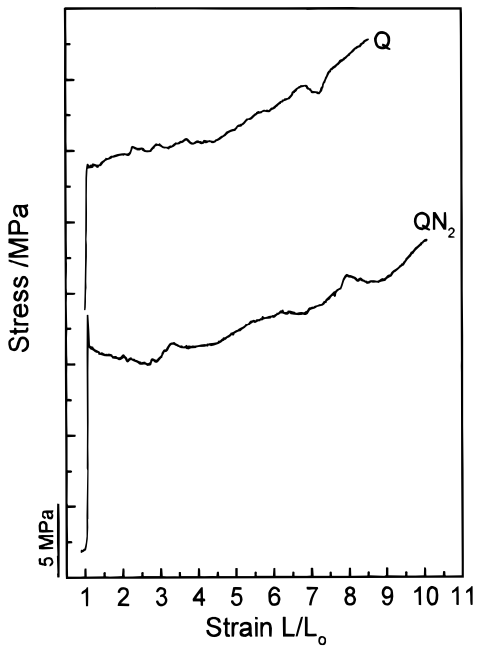

Figure 5. Stress−strain curves of $S_{51}B_{09}C_{40}$ prepared under different conditions (40 mm/min): Q = quenched in cold water; QN_2 = quenched in cold water and immersed in liquid nitrogen.

Table 4 summarize the results. $S_{57}B_{27}C_{16}$ (Q) exhibits a dramatically improved stress−strain behavior compared with $S_{57}B_{27}C_{16}$ (S), the solvent cast sample. The strain at break is approximately ∼690% and shows a defined yield point as well as a reduction of the elastic modulus to 250 MPa. $S_{51}B_{09}C_{40}$ (Q) showed a similar behavior (see Figure 5 and Table 4). These melt-pressed samples also showed necking, but the whitening was not so evident as in the solution cast samples. Figure 6 shows the electron micrograph of $S_{57}B_{27}C_{16}$ (Q) stained with OsO_4. Although the microdomains are less organized than in $S_{57}B_{27}C_{16}$ (S), the same morphology, i.e., core shell cylinders (see arrows), is formed from the melt. Because of the less pronounced stress whitening in this material (Q), we propose that the microcrazes, which are the consequence of surface stresses at internal interfaces, can only grow to a limited extent. This is a consequence of the lower degree of order in this core shell cylinder morphology. We assume that these less organized cylinders are more efficient to stop craze growth. In the solution cast material crazes probably grow along grain boundaries.

Neck formation which occurs parallel to stress whitening indicates that, simultaneously to the craze formation through cavitation in the rubber and craze propagation through the PS matrix, a plastic deformation takes place, which could be a combined deformation mechanism of the PS and PCL microdomains.

Figure 6. Transmission electron micrograph of $S_{57}B_{27}C_{16}$, which was compression molded and quenched in cold water (stained with OsO_4).

Further evidence that supports this view of the interrelation between the mechanical behavior and morphology is the stress−strain curves obtained for samples that were melt-pressed and annealed at 140 °C for 2 h (A). In this case a higher order of the microdomains can be reached with respect to samples that were only melt-pressed and quenched. A decrease of the elongation at break from ∼690% in (Q) to ∼460% in (A), along with an increase of the modulus (see Table 4), is observed.

To prove whether the semicrystalline core facilitates the rubber cavitation and consequently craze formation (probably due to the contraction that takes place during the crystallization at a temperature $T_c < T_{g(matrix)}$), the following experiment was carried out. Stress−strain experiments were performed with $S_{57}B_{27}C_{16}$ and $S_{51}B_{09}C_{40}$ samples, which were additionally immersed in liquid nitrogen (QN_2) after rapid cooling from the melt

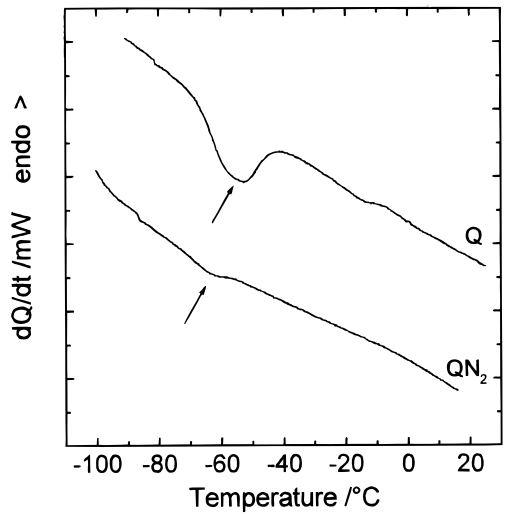

Figure 7. DSC cooling scans of $S_{57}B_{27}C_{16}$ (Q) and QN_2 recorded at −20 °C/min.

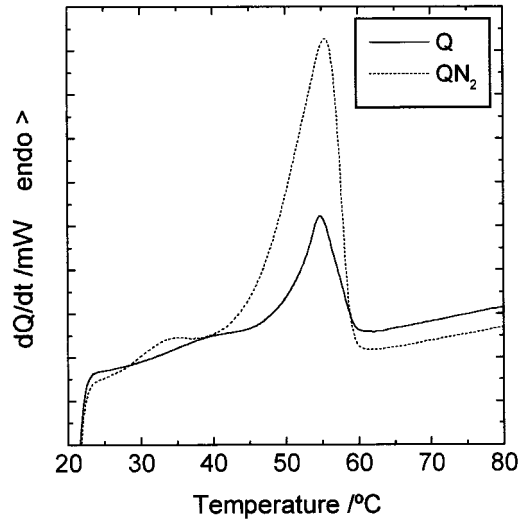

Figure 8. DSC heating scans of $S_{57}B_{27}C_{16}$ (Q) and QN_2 recorded at 20 °C/min.

to room temperature. In both cases an increase of the crystallinity occurs due to extension of the crystallization peak to temperatures below 0 °C. Moreover, $S_{57}B_{27}C_{16}$ exhibits fractionated crystallization. DSC cooling runs of $S_{57}B_{27}C_{16}$ from room temperature (see Figure 7) show a significant reduction of the size of the exotherm at −55 °C in QN_2, the liquid nitrogen quenched material. Figure 8 shows the DSC heating runs of $S_{57}B_{27}C_{16}$ (Q) and QN_2 from room temperature. The Q and QN_2 samples have crystallinities of 10% and 29%, respectively. These results confirm that additional crystallization has taken place during liquid N_2 quenching. The stress−strain behavior values for $S_{57}B_{27}C_{16}$ (QN_2) and $S_{51}B_{09}C_{40}$ (QN_2) are also included in Table 4. A higher modulus compared to Q results from the higher degree of crystallinity. The extension of these samples up to approximately 900% evidences that the high ductility of these triblock copolymers has to be attributed to the crystallinity of the core in the irregular-packed polygonal core shell cylinders. This becomes even more obvious if the stress−strain experiments of this sample are performed at 65 °C (see Figure 5, Table 4) where the PCL crystals are molten. Thus, the overall fraction of rubbery material is 40%. This is reflected in the low modulus. However, the strain at break is only about 40%. Probably transformation from polygonal to circular cylinders has taken place, so that the craze formation and propagation is no longer effective. The ultimate elongation of this material is comparable to that of PS-*b*-PB diblock copolymers with PB cylinders, but with a lower modulus. At present we can only speculate that upon melting of the cylinder core a transition from the polygonal shape, which causes a tremendous number of stress concentrations, to a simple circular cylinder occurs. This concept might be applied to other multicomponent thermoplastic materials.

Acknowledgment. This work is supported by the joint project BASF/BMFT no. 03M40861 and Stiftung Innovation Rheinland-Pfalz. V. Balsamo acknowledges financial support from CONICIT (Venezuela) through grant S1-96001934. The authors are indebted to Prof. Alejandro Müller (Universidad Simón Bolívar, Venezuela) and Prof. Andrea Lazeri (Universitá di Pisa, Italy) for valuable discussions. We are also grateful to Mr. Wurfel for assistance in the TEM work and to Dr. Voigt-Martin for giving access to the TEM equipment.

References and Notes

(1) Riess, G.; Hurtrez, G.; Bahadur, P. Block Copolymers. In *Encyclopedia of Polymer Science and Technology*; Wiley-Interscience: New York, 1984; Vol. 2.
(2) Mogi, Y.; Mori, K.; Kotsuyi, H.; Matsushita, Y.; Noda, I. *Macromolecules* **1993**, *26*, 5169.
(3) Beckmann, J.; Auschra, C.; Stadler, R. *Makromol. Chem., Rapid Commun.* **1994**, *15*, 67.
(4) Krappe, U.; Stadler, R.; Voigt-Martin, I. G. *Macromolecules* **1995**, *28*, 4558.
(5) Stadler, R.; Auschra, C.; Beckmann, J.; Krappe, U.; Voigt-Martin, I. G.; Leibler, L. *Macromolecules* **1995**, *28*, 3080.
(6) Zheng, W.; Wang, Z. G. *Macromolecules* **1995**, *28*, 7215.
(7) Breiner, U.; Abetz, V.; Krappe, U.; Stadler, R. *Macromol. Chem. Phys.* **1997**, *198*, 1051.
(8) Jung, K.; Abetz, V.; Stadler, R. *Macromolecules* **1996**, *29*, 1076.
(9) deGennes, P. G. *Macromolecules* **1980**, *13*, 1069.
(10) Semenov, A. N. *Sov. Phys., JETP* **1985**, *61*, 733.
(11) Kudose, I.; Kotaka, T. *Macromolecules* **1984**, *17*, 2325.
(12) Matsushita, Y.; Yamada, K.; Hattori, T.; Fujimoto, T.; Sawada, Y.; Nagasawa, M.; Matsui, C. *Macromolecules* **1983**, *16*, 10.
(13) Breiner, U. Doctoral dissertation, Universität Mainz, 1996.
(14) Mogi, Y.; Nomura, M.; Kotsuji, H.; Ohnishi, K.; Matsushita. Y.; Noda, I. *Macromolecules* **1994**, *27*, 6755.
(15) Jung, K.; Abetz, V.; Stadler, R.; Voigt-Martin, I. G. *Macromolecules* **1996**, *29*, 1076.
(16) Brinkmann, S.; Stadler, R.; Thomas, E. L.; Abetz, V. *Polym. Prepr.* **1997**, *38*, 1, 475.
(17) Nojima, S.; Kato, K.; Yamamoto, S.; Ashida, T. *Macromolecules* **1992**, *25*, 2237.
(18) Nojima, S.; Yamamoto, S.; Ashida, T. *Polym. J.* **1995**, *27*, 7, 673.
(19) Drewinski, M. A. *Macromol. Symp.* **1995**, *91*, 107.
(20) Balsamo, V.; von Gyldenfeldt, F.; Stadler, R. *Macromol. Chem. Phys.* **1996**, *197*, 1159.
(21) Balsamo, V.; Müller, A. J.; von Gyldenfeldt, F.; Stadler, R. *Macromol. Chem. Phys.* **1998**, *199*, 1063.
(22) Balsamo, V.; Müller, A. J.; Stadler, R. *Macromolecules* **1998**, *31*, 7756.
(23) Balsamo, V.; von Gyldenfeldt, F.; Stadler, R. *Macromol. Chem. Phys.* **1996**, *197*, 3317.
(24) Lotz, B.; Kovacs, A. J. *Polym. Prepr. (Am. Chem. Soc., Div. Polym. Chem.)* **1969**, *10* (2), 820.
(25) O'Malley, J. J.; Crystal, R. G.; Erhardt, P. F. *Polym. Prepr. (Am. Chem. Soc., Div. Polym. Chem.)* **1969**, *10* (2), 796.
(26) Santana, O. O.; Müller, A. J. *Polym. Bull. (Berlin)* **1994**, *32*, 471.
(27) Argon, A. S.; Cohen, R. E. *Adv. Polym. Sci.* **1990**, *90/91*, 301.
(28) Frensch, H.; Harnischfeger P.; Jungnickel, B. J. In *Multiphase Polymers: Blends and Ionomers*, Utracki, L. A., Weiss, R. A., Eds.; *ACS Symp. Ser.* **1989**, *101*, 395.
(29) Arnal, M. L.; Matos, M. E.; Morales, R. A.; Santana, O. O.; Müller, A. *J. Macromol. Chem. Phys.* **1998**, *199*, 2275.

(30) Argon, A. S.; Cohen, R. E.; Gebizlioglu, O. S.; Schwier, C. E. *Adv. Polym. Sci.* **1983**, *52/53*, 275.
(31) Heuschen, J.; Vion, J. M.; Jeromé, R.; Teyssié, Ph. *Macromolecules* **1989**, *22*, 2446.
(32) Kotaka, T.; Miki, T.; Arai, K. *J. Macromol. Sci. Phys.* **1980**, *B17* (2), 303.
(33) Yamaoka, I.; Kimura, M. *Polymer* **1993**, *34*, 21, 4409.
(34) Sakurai, S.; Sakamoto, J.; Shibayama, M.; Nomura, S. *Macromolecules* **1993**, *26*, 3351.
(35) Keller, A.; Odell, J. A. In *Processing Structures and Properties of Block Copolymers*; Elsevier Appl. Sci.: Amsterdam, 1985; p 29.
(36) Legge, N. R.; Holden, G.; Schroeder, H. E. *Thermoplastic Elastomers*, 1st ed.; Hanser Publishers: Munich, 1987.
(37) *Polymeric Materials Encyclopedia*; Joseph, C., Ed.; CRC Press: New York, 1996; Vol. 10, p 8002.
(38) Arai, K.; Kotaka, T.; Kitano, Y.; Yoshimura, K. *Macromolecules* **1980**, *13*, 1670.
(39) Yu, J. M.; Dubois, P.; Jèrôme, R. *Macromolecules* **1996**, *29*, 8362.
(40) Brinkmann, S. Doctoral Dissertation, Universitaet Mainz, 1998.
(41) Balsamo, V. Doctoral Dissertation, Universitaet Mainz, 1996.
(42) *Polymer Handbook*, 3rd ed.; Brandrup, J., Immergut, E. H., Eds.; J. Wiley & Sons: New York, 1989.
(43) Hubbel, D. S.; Cooper, S. L. *J. Polym. Sci., B: Polym. Phys.* **1977**, 3035.
(44) Elias, H. G. *An Introduction to Plastics*, 1st ed.; VCH: Weinheim, 1993.

MA971380K